Biomedical Optics EXPRESS

Combined reflectance confocal microscopy/optical coherence tomography imaging for skin burn assessment

Nicusor Iftimia,[1,*] R. Daniel Ferguson,[1] Mircea Mujat,[1] Ankit H. Patel,[1] Ellen Ziyi Zhang,[2] William Fox,[3] and Milind Rajadhyaksha[4]

[1]*Physical Sciences, Inc., Andover, MA 01810, USA*
[2]*Wellman Center for Photomedicine, Massachusetts General Hospital, Boston, MA 02144, USA*
[3]*Lucid Inc., Rochester, NY 14604, USA*
[4]*Dermatology Service, Memorial Sloan-Kettering Cancer Center, New York, NY 10021, USA*
**iftimia@psicorp.com*

Abstract: A combined high-resolution reflectance confocal microscopy (RCM)/optical coherence tomography (OCT) instrument for assessing skin burn gravity has been built and tested. This instruments allows for visualizing skin intracellular details with submicron resolution in the RCM mode and morphological and birefringence modifications to depths on the order of 1.2 mm in the OCT mode. Preliminary testing of the dual modality imaging approach has been performed on the skin of volunteers with some burn scars and on normal and thermally-injured Epiderm FTTM skin constructs. The initial results show that these two optical technologies have complementary capabilities that can offer the clinician a set of clinically comprehensive parameters: OCT helps to visualize deeper burn injuries and possibly quantify collagen destruction by measuring skin birefringence, while RCM provides submicron details of the integrity of the epidermal layer and identifies the presence of the superficial blood flow in the upper dermis. Therefore, the combination of these two technologies within the same instrument may provide a more comprehensive set of parameters that may help clinicians to more objectively and nonivasively assess burn injury gravity by determining tissue structural integrity and viability.

OCIS codes: (170.0170) Medical optics and biotechnology; (170.4580) Optical diagnostics for medicine; (180.1790) Confocal microscopy; (180.1655) Coherence tomography; (170.6935) Tissue characterization.

References and links

1. Burn incidence fact sheet (American Burn Association 2011). http://www.ameriburn.org/resources_factsheet.php
2. P. A. Brigham and E. McLoughlin, "Burn incidence and medical care use in the United States: estimates, trends, and data sources," J. Burn Care Rehabil. **17**(2), 95–107 (1996).
3. R. Walls, J. J. Ratey, and R. I. Simon, *Rosen's Emergency Medicine: Expert Consult Premium Edition - Enhanced Online Features and Print (Rosen's Emergency Medicine: Concepts & Clinical Practice (2v.))* (Mosby, 2009).
4. D. Church, S. Elsayed, O. Reid, B. Winston, and R. Lindsay, "Burn wound infections," Clin. Microbiol. Rev. **19**(2), 403–434 (2006).
5. M. S. Arons, "Burn wound infection—a review," Conn. Med. **29**(10), 718–722 (1965).
6. N. Agnihotri, V. Gupta, and R. M. Joshi, "Aerobic bacterial isolates from burn wound infections and their antibiograms—a five-year study," Burns **30**(3), 241–243 (2004).
7. D. J. Dries, "Management of burn injuries—recent developments in resuscitation, infection control and outcomes research," Scand. J. Trauma Resusc. Emerg. Med. **17**(1), 14–27 (2009).
8. R. M. Johnson and R. Richard, "Partial-thickness burns: identification and management," Adv. Skin Wound Care **16**(4), 178–187 (2003).
9. B. S. Atiyeh, S. W. Gunn, and S. N. Hayek, "State of the art in burn treatment," World J. Surg. **29**(2), 131–148 (2005).

#184392 - $15.00 USD Received 29 Jan 2013; revised 13 Mar 2013; accepted 18 Mar 2013; published 8 Apr 2013

10. A. M. Watts, M. P. Tyler, M. E. Perry, A. H. Roberts, and D. A. McGrouther, "Burn depth and its histological measurement," Burns **27**(2), 154–160 (2001).
11. A. C. Roth, J. C. Reid, C. L. Puckett, and M. J. Concannon, "Digital images in the diagnosis of wound healing problems," Plast. Reconstr. Surg. **103**(2), 483–486 (1999).
12. O. C. Jones, D. I. Wilson, and S. Andrews, "The reliability of digital images when used to assess burn wounds," J. Telemed. Telecare **9**(Supplement 1), 22–24 (2003).
13. L. Roa, T. Gómez-Cía, B. Acha, and C. Serrano, "Digital imaging in remote diagnosis of burns," Burns **25**(7), 617–623 (1999).
14. Z. B. Niazi, T. J. Essex, R. Papini, D. Scott, N. R. McLean, and M. J. Black, "New laser Doppler scanner, a valuable adjunct in burn depth assessment," Burns **19**(6), 485–489 (1993).
15. M. G. Sowa, L. Leonardi, J. R. Payette, J. S. Fish, and H. H. Mantsch, "Near infrared spectroscopic assessment of hemodynamic changes in the early post-burn period," Burns **27**(3), 241–249 (2001).
16. L. Leonardi, M. G. Sowa, J. R. Payette, and H. H. Mantsch, "Near-infrared spectroscopy and imaging: a new approach to assess burn injuries," Am. Clin. Lab. **19**(8), 20–22 (2000).
17. J. M. Still, E. J. Law, K. G. Klavuhn, T. C. Island, and J. Z. Holtz, "Diagnosis of burn depth using laser-induced indocyanine green fluorescence: a preliminary clinical trial," Burns **27**(4), 364–371 (2001).
18. J. Micheels, B. Aisbjorn, and B. Sorensen, "Laser doppler flowmetry. A new non-invasive measurement of microcirculation in intensive care?" Resuscitation **12**(1), 31–39 (1984).
19. D. H. Park, J. W. Hwang, K. S. Jang, D. G. Han, K. Y. Ahn, and B. S. Baik, "Use of laser Doppler flowmetry for estimation of the depth of burns," Plast. Reconstr. Surg. **101**(6), 1516–1523 (1998).
20. A. J. Holland, H. C. Martin, and D. T. Cass, "Laser Doppler imaging prediction of burn wound outcome in children," Burns **28**(1), 11–17 (2002).
21. T. J. O'Reilly, R. J. Spence, R. M. Taylor, and J. J. Scheulen, "Laser Doppler flowmetry evaluation of burn wound depth," J. Burn Care Rehabil. **10**(1), 1–6 (1989).
22. L. Atiles, W. Mileski, G. Purdue, J. Hunt, and C. Baxter, "Laser Doppler flowmetry in burn wounds," J. Burn Care Rehabil. **16**(4), 388–393 (1995).
23. M. A. Altintas, A. A. Altintas, K. Knobloch, M. Guggenheim, C. J. Zweifel, and P. M. Vogt, "Differentiation of superficial-partial vs. deep-partial thickness burn injuries in vivo by confocal-laser-scanning microscopy," Burns **35**(1), 80–86 (2009).
24. D. Terhorst, A. Maltusch, E. Stockfleth, S. Lange-Asschenfeldt, W. Sterry, M. Ulrich, and B. Lange-Asschenfeldt, "Reflectance confocal microscopy for the evaluation of acute epidermal wound healing," Wound Repair Regen. **19**(6), 671–679 (2011).
25. Q. H. Le, W. T. Wang, J. X. Hong, X. H. Sun, T. Y. Zheng, W. Q. Zhu, and J. J. Xu, "An in vivo confocal microscopy and impression cytology analysis of goblet cells in patients with chemical burns," Invest. Ophthalmol. Vis. Sci. **51**(3), 1397–1400 (2010).
26. S. Jiao, W. Yu, G. Stoica, and L. V. Wang, "Contrast mechanisms in polarization-sensitive Mueller-matrix optical coherence tomography and application in burn imaging," Appl. Opt. **42**(25), 5191–5197 (2003).
27. M. C. Pierce, R. L. Sheridan, B. Hyle Park, B. Cense, and J. F. de Boer, "Collagen denaturation can be quantified in burned human skin using polarization-sensitive optical coherence tomography," Burns **30**(6), 511–517 (2004).
28. S. M. Srinivas, J. F. de Boer, H. Park, K. Keikhanzadeh, H. E. Huang, J. Zhang, W. Q. Jung, Z. Chen, and J. S. Nelson, "Determination of burn depth by polarization-sensitive optical coherence tomography," J. Biomed. Opt. **9**(1), 207–212 (2004).
29. M. Todorović, S. Jiao, J. Ai, D. Pereda-Cubián, G. Stoica, and L. V. Wang, "In vivo burn imaging using Mueller optical coherence tomography," Opt. Express **16**(14), 10279–10284 (2008).
30. K. H. Kim, M. C. Pierce, G. Maguluri, B. H. Park, S. J. Yoon, M. Lydon, R. Sheridan, and J. F. de Boer, "In vivo imaging of human burn injuries with polarization-sensitive optical coherence tomography," J. Biomed. Opt. **17**(6), 066012 (2012).
31. A. T. Yeh, B. Kao, W. G. Jung, Z. Chen, J. S. Nelson, and B. J. Tromberg, "Imaging wound healing using optical coherence tomography and multiphoton microscopy in an in vitro skin-equivalent tissue model," J. Biomed. Opt. **9**(2), 248–253 (2004).
32. D. H. Park, J. W. Hwang, K. S. Jang, D. G. Han, K. Y. Ahn, and B. S. Baik, "Use of laser Doppler flowmetry for estimation of the depth of burns," Plast. Reconstr. Surg. **101**(6), 1516–1523 (1998).
33. E. J. Droog, W. Steenbergen, and F. Sjöberg, "Measurement of depth of burns by laser Doppler perfusion imaging," Burns **27**(6), 561–568 (2001).
34. A. J. Holland, H. C. Martin, and D. T. Cass, "Laser Doppler imaging prediction of burn wound outcome in children," Burns **28**(1), 11–17 (2002).
35. L. Atiles, W. Mileski, G. Purdue, J. Hunt, and C. Baxter, "Laser Doppler flowmetry in burn wounds," J. Burn Care Rehabil. **16**(4), 388–393 (1995).
36. S. A. Pape, C. A. Skouras, and P. O. Byrne, "An audit of the use of laser Doppler imaging (LDI) in the assessment of burns of intermediate depth," Burns **27**(3), 233–239 (2001).
37. V. J. Anselmo and B. E. Zawacki, "Multispectral photographic analysis. A new quantitative tool to assist in the early diagnosis of thermal burn depth," Ann. Biomed. Eng. **5**(2), 179–193 (1977).
38. L. T. Vo, P. Anikijenko, W. J. McLaren, P. M. Delaney, D. H. Barkla, and R. G. King, "Autofluorescence of skin burns detected by fiber-optic confocal imaging: evidence that cool water treatment limits progressive thermal damage in anesthetized hairless mice," J. Trauma **51**(1), 98–104 (2001).

#184392 - $15.00 USD Received 29 Jan 2013; revised 13 Mar 2013; accepted 18 Mar 2013; published 8 Apr 2013

39. S. M. Milner, S. Bhat, S. Gulati, G. Gherardini, C. E. Smith, and R. J. Bick, "Observations on the microcirculation of the human burn wound using orthogonal polarization spectral imaging," Burns **31**(3), 316–319 (2005).
40. B. W. Graf and S. A. Boppart, "Multimodal *in vivo* skin imaging with integrated optical coherence and multiphoton microscopy," IEEE J. Sel. Top. Quantum Electron. **18**(4), 1280–1286 (2012).
41. http://www.millipore.com/catalogue/item/ct02?cid=bios-x-goog-1007-9999-rc
42. J. Thomsen, N. Bendsoe, K. Svanberg, S. Andersson-Engels, T. M. Jorgensen, L. Thrane, H. E. Larsen, F. Pedersen, and P. E. Andersen, "Optical Doppler tomography for monitoring vascularization during photodynamic therapy of skin cancer lesions," Proc. SPIE **6991**, 699118, 699118-7 (2008).
43. Y. Zhao, Z. Chen, C. Saxer, S. Xiang, J. F. de Boer, and J. S. Nelson, "Phase-resolved optical coherence tomography and optical Doppler tomography for imaging blood flow in human skin with fast scanning speed and high velocity sensitivity," Opt. Lett. **25**(2), 114–116 (2000).
44. B. J. Vakoc, R. M. Lanning, J. A. Tyrrell, T. P. Padera, L. A. Bartlett, T. Stylianopoulos, L. L. Munn, G. J. Tearney, D. Fukumura, R. K. Jain, and B. E. Bouma, "Three-dimensional microscopy of the tumor microenvironment in vivo using optical frequency domain imaging," Nat. Med. **15**(10), 1219–1223 (2009).
45. L. An, J. Qin, and R. K. Wang, "Ultrahigh sensitive optical microangiography for in vivo imaging of microcirculations within human skin tissue beds," Opt. Express **18**(8), 8220–8228 (2010).
46. J. Qin, J. Jiang, L. An, D. Gareau, and R. K. Wang, "In vivo volumetric imaging of microcirculation within human skin under psoriatic conditions using optical microangiography," Lasers Surg. Med. **43**(2), 122–129 (2011).
47. E. Z. Zhang and B. J. Vakoc, "Polarimetry noise in fiber-based optical coherence tomography instrumentation," Opt. Express **19**(18), 16830–16842 (2011).
48. D. Stifter, E. Leiss-Holzinger, Z. Major, B. Baumann, M. Pircher, E. Götzinger, C. K. Hitzenberger, and B. Heise, "Dynamic optical studies in materials testing with spectral-domain polarization-sensitive optical coherence tomography," Opt. Express **18**(25), 25712–25725 (2010).
49. E. Z. Zhang, W. Y. Oh, M. L. Villiger, L. Chen, B. E. Bouma, and B. J. Vakoc, "Numerical compensation of system polarization mode dispersion in polarization-sensitive optical coherence tomography," Opt. Express **21**(1), 1163–1180 (2013).

1. Introduction

Skin burns are one of the most common and devastating forms of trauma. Data from the American Burn Association show that over 450,000 people received treatment in the US in 2011 after burn injury [1,2]. The severity of the burns ranges from a mild first-degree burn, affecting only the epidermal layer, to second degree burns affecting both epidermis and dermis, and full-thickness burns requiring skin grafting [3]. Figure 1 provides a schematic representation of the skin layers in relation to the depth of burn injury.

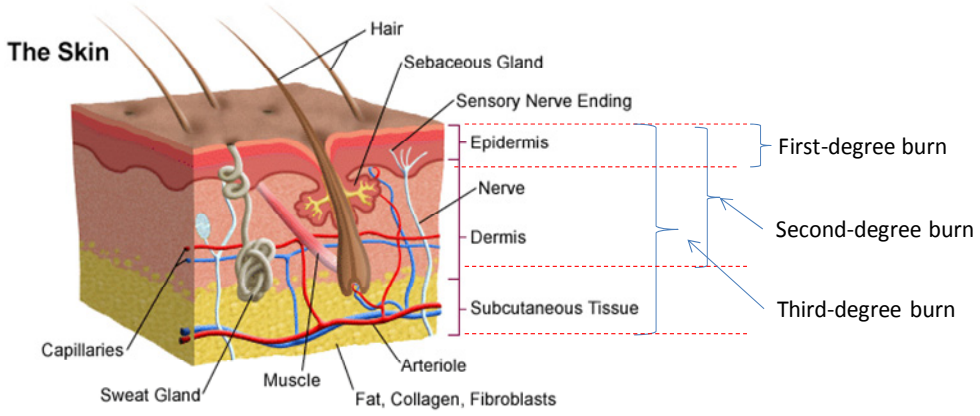

Fig. 1. Basic skin anatomy, showing the depth of injury for first-, second-, and third-degree burns. Source: http://www.childrenshospital.org/az/Site784/mainpageS784P0.html (modified and reprinted with permission).

Burn wound depth is a major determinant of patient treatment and morbidity. While superficial first degree burns generally heal by re-epithelialization with minimal or no scarring, deeper wounds can form hypertrophic or contracted scars, often requiring surgical

#184392 - $15.00 USD Received 29 Jan 2013; revised 13 Mar 2013; accepted 18 Mar 2013; published 8 Apr 2013

excision and grafting to prevent a suboptimal result. A typical feature of these burns is the high rate of infection, which necessitates long periods of hospitalization. Significant thermal injuries induce a state of immunosuppression that predisposes burn patients to infectious complications [4–6]. Therefore, patients with serious second or third degree burns require immediate specialized care in order to minimize morbidity and mortality [7]. Often, prompt referral to burn centers is needed for patients with major burns to improve burn outcomes.

Rapid and accurate assessment of burn wound depth is a priority in treating burn-injured patients. Clinical evaluation is the most widely employed and cost-effective method of assessing burn wound depth and tissue viability [8,9]. This method is based on the subjective assessment of visual and tactile characteristics of a burn wound, namely appearance, capillary blanching and refill, capillary staining, and sensibility to light touch and pinprick [10]. Unfortunately, burn severity assessment by clinical evaluation alone is still governed largely by subjective criteria. To aid clinical evaluation, digital photography is often been used for assessment at the bedside [11–13]. However, digital imaging as a method of assessing burn wound depth has major limitations. First, the accuracy is widely considered to be suboptimal. Overall estimates report that the assessment is accurate in about two thirds of cases, with the most frequent cause of error attributed to overestimation [14]. Second, reliability is questionable and considerable variation exists between assessments made by different clinicians. In addition, the extent of tissue damage may not be immediately visually apparent with digital imaging.

Efforts for increasing objectivity in burn depth assessment have been widespread in recent years and include use of visible or near-infrared light spectroscopy [15,16], fluorescent imaging [16,17], laser Doppler techniques [18–22], and more recently confocal microscopy (CM) [23–25], optical coherence tomography (OCT) [26–30], and multiphoton microscopy (MPM) [31].

Laser Doppler flowmetry (LDF) and laser Doppler perfusion imaging (LDPI) are the oldest Doppler-based techniques used for burn depth estimation [32,33]. They are both based on the Doppler principle. The LDF technique uses a fiber-optic probe in direct contact with the burn wound. This technique assesses microcirculation 1 mm below the point of probe-tissue contact. The accuracy of flowmetry in burn depth diagnosis ranges from 90% to 97%, as compared to 66% with clinical evaluation alone [34,35]. Despite this very high accuracy, technical limitations render flowmetry to be still a suboptimal technique because it measures perfusion in one spot at a time, and therefore the procedure is relatively time consuming [36]. Laser Doppler imaging (LDI) and laser Doppler perfusion imaging (LDPI) seem to overcome the limitations of flowmetry by allowing measurements over relatively large areas. After scanning a burned area, LDI devices generate a color-coded perfusion map that corresponds to varying burn depths. LDI is a highly valid measure of burn wound depth, and its accuracy has been reported at up to 99%. However, this is valid only if infected and highly blistering wounds are excluded [36]. The major limitation of LDI and LDPI is that their accuracy can be affected by the heterogeneity and curvature of tissues, thickness of topical wound dressings, and ambient light and temperature, as well as pathophysiological effects of skin color, blisters, and wound fluids. In addition, wound infection can adversely affect depth measurements.

Reflection-optical multispectral imaging has also been tested for burn assessment [37]. The spectroscopic approach consists of acquiring spectra and comparison using multivariate analysis to determine diagnostic regions of the spectra. However, the reflected light from necrotic tissue, scarring, and dermal vessel oxygen saturation alter the results of the measurements. Clinical prototypes are currently being used in various burn centers in an effort to determine clinical validity.

Optical coherence tomography (OCT) has been applied with success to burn injury characterization [26–30]. The polarization-sensitive version of OCT measures the extent to which reflected light from burns has changed its polarization. Thus, it provides polarimetric measurements of birefringence amplitude, orientation, and diattenuation to assess tissue

#184392 - $15.00 USD Received 29 Jan 2013; revised 13 Mar 2013; accepted 18 Mar 2013; published 8 Apr 2013

structure and function, which are very helpful for wound depth characterization [27]. Reduction in collagen birefringence is thought to be related to burn depth. However, superficial burns in the epidermal layer cannot be reliably evaluated with OCT because of insufficient resolution to resolve individual cells and reliably determine tissue damage. Also, skin perfusion cannot be reliably measured with OCT.

Both fluorescence and reflectance confocal microscopy (CM) have been evaluated as well for burn gravity assessment [23–25]. Illumination of tissue with blue light causes autofluorescence that is directly proportional to the burn depth [38]. It is thought that the mechanism of autofluorescence is related to the presence of denatured collagen or other cellular proteins. Unfortunately, the imaging depth of CM is limited to a few hundred of microns (max 300 μm in skin), and therefore CM cannot reliably determine burn depth in the dermal layer, especially when the wound depth is over several hundred of microns.

Orthogonal polarization spectral imaging (OPSI) is another technique that is being studied for skin burn measurements [39]. With this technique the tissue is illuminated with linearly polarized light within the hemoglobin spectrum and the image is acquired in the orthogonal polarization channel. OPSI has been tested for the noninvasive assessment of skin microcirculation through the surface of the human burn wound [39]. Two distinct microcirculatory patterns were seen in burned skin with this technique: superficial burns had small visible dermal capillaries studded throughout the field of view, while deep burns showed large thrombosed vessels coursing in a crisscrossed fashion. This disparity reflects the marked difference between the mean optical densities for superficial burns and deep burns. Although OPSI is a promising technology, it still has not been yet FDA approved for clinical use.

All these studies suggest that many of the researched technologies, when used alone, offer some benefits but along with some limitations. Interestingly, the benefits may be synergistically combined into complementary capabilities. For example, microscopy techniques visualize cellular-level detail at high resolution in the superficial layers of tissues, but fail to visualize deeper layers and thus cannot measure burn depth. Other techniques, like OCT, provide deeper imaging and measurement of depth albeit with structural-level detail at lower resolution. Therefore, it may be speculated that the combination of two or more complementary technologies within the same instrument might overcome the limitations of each and help to more reliably diagnosis. Recently, optical coherence microscopy (OCM) was integrated with multiphoton microscopy (MPM) within the same instrument with the goal of combining the capabilities of OCM reflectance imaging with those of MPM autofluorescence imaging, and thus helping, in addition to structural imaging, to visualize the intra-cytoplasmic distribution of proteins (keratin) and pigment (melanin) in skin [40].

In this paper we show that two imaging modalities, reflectance confocal microscopy (RCM) and polarization sensitive OCT (PSOCT), when combined within the same instrument, can provide a more complete set of parameters that might help clinicians to better assess burn injury gravity. The preliminary testing of this approach in a skin model and normal/burn scar skin of the volunteers is discussed.

2. Materials and methods

2.1 Instrument development

An advanced RCM/OCT benchtop instrument was developed with the goal of testing the hypothesis that combined RCM/OCT imaging may enable more comprehensive and more reliable evaluation of skin burns. The dual modality instrument (see simplified schematic in Fig. 2) consists of four subsystems: OCT subsystem, RCM subsystem, common path RCM/OCT imaging probe, and Instrument Control unit.

The OCT subsystem is based on a fiber-optic interferometer (10/90 fiber splitter with, 2 circulators, a 50/50 fiber combiner, and reference/sample arm optics) and a dual polarization-

#184392 - $15.00 USD Received 29 Jan 2013; revised 13 Mar 2013; accepted 18 Mar 2013; published 8 Apr 2013

sensitive (PS) balanced detector (Model INT-POL-1300, Thorlabs, NJ). This subsystem uses a polygon-based wavelength sweeping light source (Model HS 2000 SANTEC, Japan), with a 1310 nm central wavelength and 125 nm bandwidth. According to Eq. (1), the theoretical axial sectioning resolution l_z provided by this source is about 6 μm in air and 4.5 μm in tissue:

$$l_z = 0.44\frac{\lambda_0^2}{\bar{n}\Delta\lambda}, \tag{1}$$

where λ_0 is the center wavelength of the light source, $\Delta\lambda$ is the spectral width of the light source, and n is the refractive index of the sample (~1.34 for biological tissues).

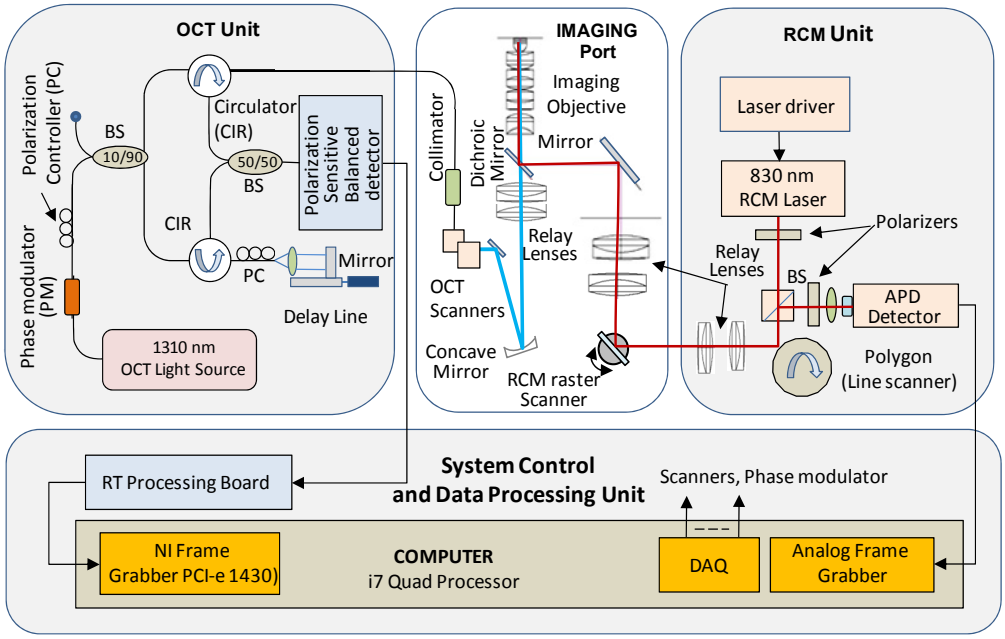

Fig. 2. Schematic of the RCM/OCT instrument.

To obtain both structural and birefringence data, the sample is probed with two orthogonal polarization states of the light. Therefore, a phase modulator (Model 4423, New Focus) is used to change the polarization status of the light, while a polarization sensitive balanced detector is used for fringe-signal detection. The PS analysis method for the PS-OCT data is based on Jones matrix analysis published by other investigators [27].

The RCM subsystem is based on a breadboard setup from Lucid, Inc. (Rochester, NY), which was modified to allow for combining both RCM and OCT beams within the same optical path and imaging through a high magnification objective. It uses a polygon scanner (Lincoln Lasers) to generate the high-speed line scan and a Cambridge Technology galvanometer to generate the low speed raster scan. An 830 nm laser beam (computer adjustable within the 0-20 mW range) is used for sample illumination. The backscattered light is de-scanned and detected with an avalanche photodiode. A specialized custom designed board is used to control the scanners, the laser diode, and the photodetector. A frame-grabber that resides inside the computer is used to digitize the acquired signal and generate an image of the sample.

The common path imaging probe (see optical design in Fig. 3) uses a dichroic mirror to combine the OCT and RCM beams within the same optical path. The main reason for using a folded optical path was to avoid the use of the dichroic mirror in the reflection mode for OCT. The dichroic mirrors are known to insert significant dispersion and thus degrade the quality of

#184392 - $15.00 USD Received 29 Jan 2013; revised 13 Mar 2013; accepted 18 Mar 2013; published 8 Apr 2013

the OCT image. A scanning engine, consisting of a pair of galvanometric mirrors, is used to generate the OCT raster scan. Since the two galvanometers have to be relayed to the pupil of the instrument imaging objective, a set of achromatic lenses and a concave turning mirror have been used to build the optical relay system.

One of the challenging tasks here was to obtain a reasonable field of view (FOV) and imaging depth in the OCT mode when a high numerical aperture (NA = 0.85) imaging objective is used in the sample arm. Our goal was to obtain a FOV in the order of 2 mm and over 1 mm imaging depth. The adopted solution here to meet these goals was to underutilize the NA of the imaging objective in the OCT mode by using a beam diameter of only 0.5 mm. Optical Zemax design was performed to optimize the optical imaging path and to ensure optimum performance for both the OCT and RCM modes. As observed (see schematic and spot diagram in Fig. 3), an Airy radius of 8.57 µm was obtained for the OCT beam, which was considered sufficient for generating a high-quality OCT image. As normal, this spot becomes larger while moving away from the focal plane. However, most of the energy is still concentrated within the Airy disk at 400 µm away from the imaging plane. With a small compromise on the lateral resolution, over 1 mm imaging range is possible with this design.

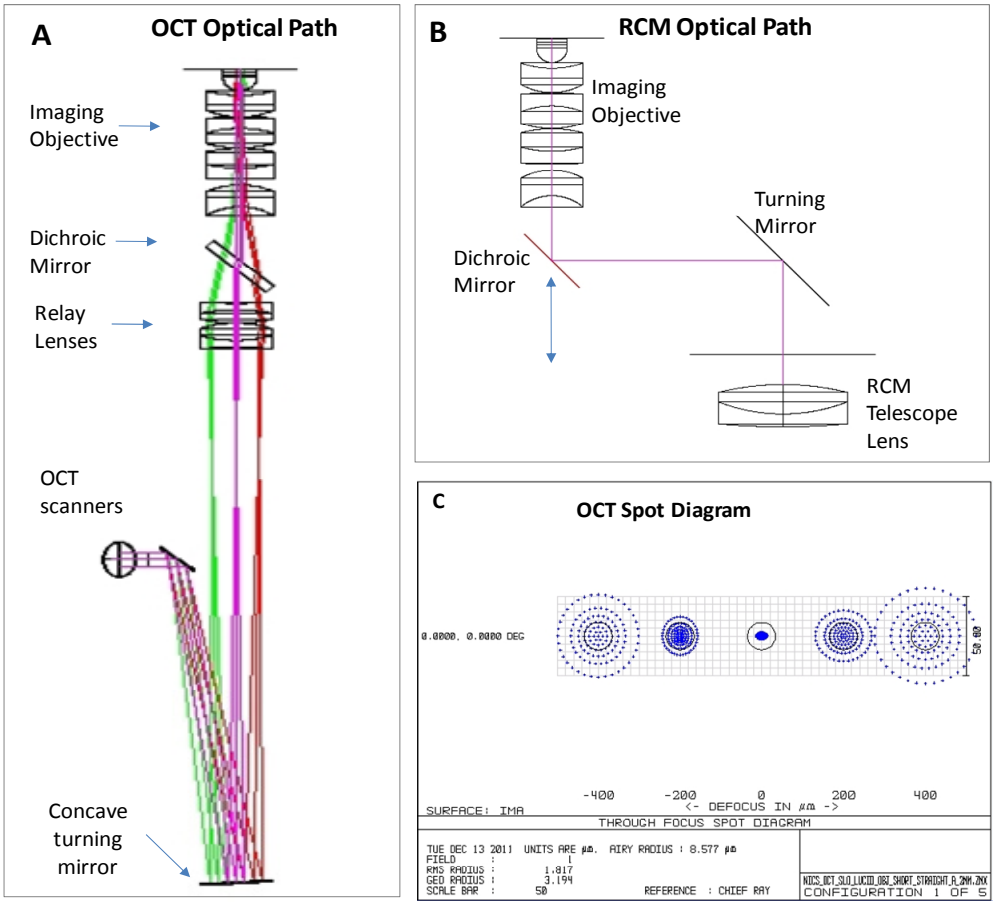

Fig. 3. Optical imaging port of the RCM/OCT instrument. (**A, B**): Zemax design of the common path optical imaging channel of the RCM/OCT instrument. (**C**): Through focus spot diagram of the OCT channel.

The system control and data processing unit consists of a quad-core computer, a real-time digital signal processing (RT-DSP) unit based on field-programmable gated-array (FPGA) hardware, which allows for OCT data processing and display at high frame rates, and

#184392 - $15.00 USD Received 29 Jan 2013; revised 13 Mar 2013; accepted 18 Mar 2013; published 8 Apr 2013

controllers for the OCT scanning engine. The RT-DSP board is a Physical Sciences, Inc. (PSI) custom design and it performs all the time consuming signal processing steps for the OCT data (FFT transform, linear interpolation, and dispersion compensation). This board operates as a standalone device that communicates with the host computer via the PCI bus. Using this board and a regular off-the-shelf computer, OCT display rates up to 40 fps are possible at an image resolution of 512x1024 pixels.

The photograph of the RCM/OCT benchtop instrument developed by PSI is shown in Fig. 4. The RCM and OCT hardware is placed on two stacked breadboards. The OCT imaging port is integrated into the RCM system, as shown in more detail in Figs. 4B, 4C, & 4D. As discussed above, folding optics is used to combine the RCM and OCT imaging paths into the same imaging objective.

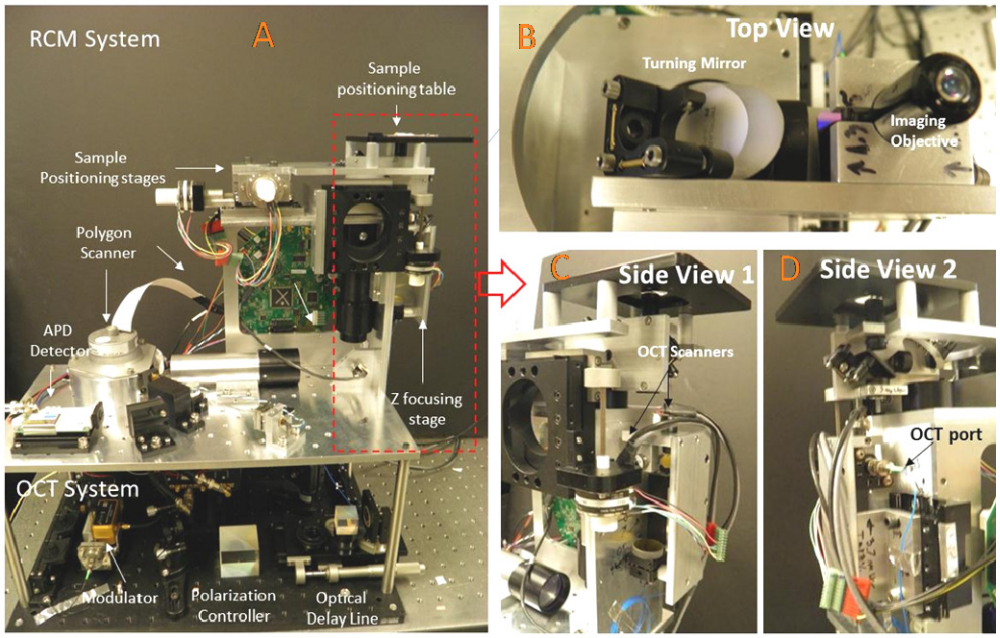

Fig. 4. (**A**): Photograph of the RCM/OCT imaging instrument. (**B**): Top view of the imaging probe. (**C,D**): Side views of the imaging probe.

2.2 Instrument characterization

This instrument was fully tested before performing measurements on the skin of the investigators (palm area) and on skin tissue constructs. Co-localization of the RCM/OCT images, imaging depth, sensitivity decay within the imaging range, field of view (FOV), and imaging resolution were measured.

Image co-localization was tested using an USAF 1951 resolution target. As observed in Figs. 5A & 5B, the same feature of the resolution target (number "6" from group 4) was visualized in both RCM and OCT modes. 3D rendering was performed on the OCT raster scan data to obtain enface OCT images of this target.

The axial resolution of OCT was determined by measuring the coherence function when a partially reflecting target (microscope cover slip) was paced in the sample arm of the OCT system. An axial resolution of about 7 μm was obtained in air, which corresponds to about 5.23 μm in tissue, while a lateral resolution on the order of 17 μm was measured using the USAF 1951 resolution target (the lines from group 4 were fully resolved). The relatively small discrepancy between the experimental and theoretical axial resolution was attributed to imperfect compensation of the dispersion between the two arms of the OCT interferometer.

#184392 - $15.00 USD Received 29 Jan 2013; revised 13 Mar 2013; accepted 18 Mar 2013; published 8 Apr 2013

The lateral resolution of the RCM channel mode was measured using a high resolution target, USAF 1951-1X. As observed in Fig. 5C, better than 1 μm lateral resolution was obtained. The 2nd element of the group 9, which has a line width of 0.87 μm, was fully resolved.

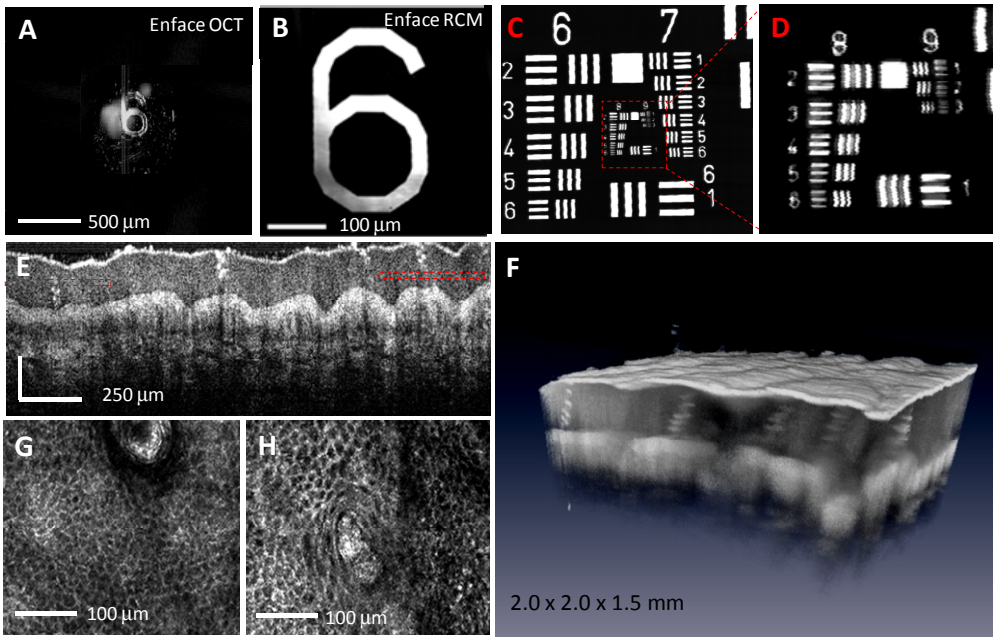

Fig. 5. (**A**): Enface OCT image of a 2 x 2 mm area from the resolution target. (**B**)**:** Co-localized RCM image. (**C-D**): RCM images of the high-resolution UASF 1951 target. (**E**): Cross-sectional OCT image OCT of the thumb area. (**F**): 3D rendering of an OCT raster scan. (**G,H**): Enface RCM images of two skin areas marked in red in (E).

Measurements on the palm of a volunteer were performed to determine instrument capability for resolving the morphology of the skin with OCT, as well as sub-cellular entities with RCM. OCT was capable to fully resolve both layers of the skin and visualize small morphological details, such as sweat glands (see Fig. 5E). 3D rendering was used to obtain the volumetric image shown in Fig. 5F. An imaging depth of over 1.2 mm and about 2 x 2 mm FOV were measured in the OCT mode. The RCM images in the two red-marked areas in the OCT frame (see Figs. 5G & 5H) demonstrate instrument capability for resolving sub-cellular features (polygonal epithelial cells with dark nuclei surrounded by a bright cytoplasm). A FOV of 420 x 420 μm with about 200 μm imaging depth was measured in the RCM mode.

The sensitivity of both RCM and OCT was measured by using a mirror in the sample arm and attenuating the signal with neutral density (ND) filters to avoid detector saturation. A sensitivity of 112 dB was measured in the OCT mode and 60 dB in the RCM mode. All these results are in a good agreement with our design predictions.

3. Results

3.1. Instrument evaluation on EpiDermFT™ skin tissue constructs

The EpiDermFT Skin Model developed by MatTech simulates human tissue with high fidelity. EpiDermFT is a normal (non-transformed), human cell-derived, metabolically active, 3D organotypic in vitro skin model. It mimics human skin, both structurally and biochemically in a reproducible manner. Therefore, this skin model is well suited to mimic minor injuries and evaluate RCM-OCT capability for monitoring changes in tissue morphology.

#184392 - $15.00 USD Received 29 Jan 2013; revised 13 Mar 2013; accepted 18 Mar 2013; published 8 Apr 2013

Acquisition and analysis of RCM and OCT images: The specimens were kept metabolically active in a small bioreactor that contained a nutrient medium provided by MatTech. Measurements were first performed on metabolically–active specimens and then on specimens that were exposed to elevated temperature (heat gun at 75°C). After heating, the specimen was put back in the incubator for 24 hours and then imaged.

An example of combined OCT/RCM measurements on normal, metabolically active specimen is shown in Fig. 6.

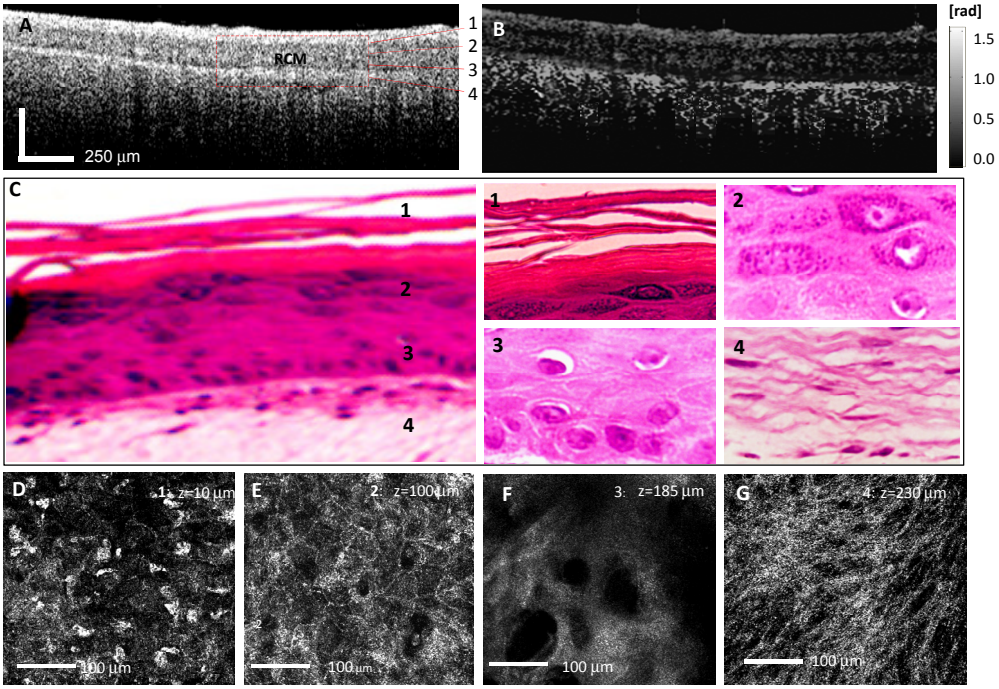

Fig. 6. Cross-sectional OCT and en face RCM images of the EpiDermFT Skin Model. (**A**): Cross-sectional OCT image; all three layers (corneum, epidermal, and dermal) were resolved by OCT. (**B**): PS OCT image showing some moderate birefringence of the dermal layer. (**C**): Histology showing the detailed morphology of the skin layers. 100x magnified images show the cobblestone cells in the corneum, larger cells with visible nuclei in the epidermis, and the collagen fibers in the dermis. (**D-G):** RCM images showing tissue morphology at different depths: Cobblestone appearance of the corneum layer (D), polygonal cells in the epidermis (E), Dermal papillae at the dermal-epidermal junction (F), and collagen fibers in the upper dermis (G).

Cross-sectional OCT imaging (see Fig. 6A) displayed the stratum corneum and the epidermal/dermal layers. The thickness of the epidermal layer was less than 200 µm, while the stratum corneum was about 50 µm, which seems to be larger than in the human skin. The presence of the collagen fibers was also noted in the phase retardance image (see Fig. 6B). However, since these fibers were not well aligned, as indicated by RCM imaging (see Fig. 6G), the birefringence was only moderate. RCM imaging also showed a notable difference between the skin construct layers. The top stratum corneum layer showed a cobblestone appearance of the cells (see Fig. 6D), similar to that seen in the 100x histology detail from Fig. 6C(1), while between 50 and 100 µm depth, the epidermal cells had a polygonal appearance (see Fig. 6E), very similar to the polygonal cell structure found in the human skin. These cells can be easily recognized in the 100x histology detail shown in Figs. 6C(2) & 6C(3). The dermal papillae cannot be recognized in the histology slide because the tissue was cut in the vertical plane. However, RCM picked-up relatively well the papillae (see Fig. 6F). Since RCM imaging depth was not sufficient to resolve the dermal layer, the RCM image

#184392 - $15.00 USD Received 29 Jan 2013; revised 13 Mar 2013; accepted 18 Mar 2013; published 8 Apr 2013

shown in Fig. 6G was obtained after shaving the epidermal layer with a razorblade. The collagen fiber can be easily identified in this figure, and the morphology correlates well with histology (see Fig. 6C(4)).

Notable changes in tissue morphology were observed after exposing the specimen to heat, as shown in Fig. 7.

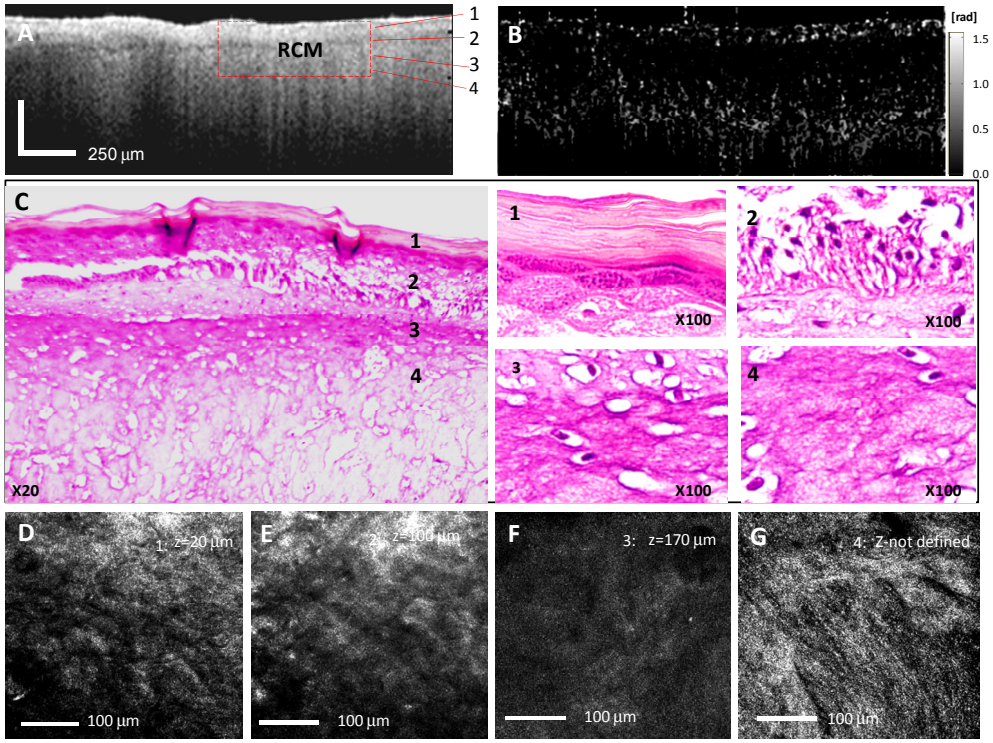

Fig. 7. Cross-sectional OCT and en face RCM images of the EpiDermFT Skin Model after injury. (**A**): OCT image. (**B**): PS OCT image showing very low birefringence of the dermal layer. (**C**): Histology confirming tissue degradation at all depths; cells are no longer differentiated. (**D-G**)**:** RCM images showing tissue morphology at different depths. The heat has killed the cells and neither the cobblestone appearance of the corneum layer (D) and the polygonal shape of the epidermal cells (E), or the dermal papillae (F) and collagen fibers in the upper dermis (G) are well distinguishable.

The dermal-epidermal junction was no longer differentiated in the OCT image after just 3 sec of exposure to heat (see Fig. 7A), while after 10 sec of exposure the epidermis started to lift up and small bubbles of fluid start to build up between the dermis and epidermis, similar to the human skin blistering after thermal injury. The RCM images showed a degradation of all layers. The excessive heat seems to have killed the cells and therefore neither the cobblestone appearance of the corneum layer (see Fig. 7D), nor the polygonal shape of the epidermal cells (see Fig. 7E), nor the dermal papillae (see Fig. 7F) were well distinguishable as on the healthy tissue. These findings are confirmed by histology results (see Figs. 7C(1-3)), which do not longer show well differentiated cells in the stratus corneus and epidermis. The collagen structure was affected as well, as indicated by both RCM and histology (see Figs. 7G and 7C(4)). Although some collagen fibers can still be seen, there is no clear differentiation between these fibers as it is was observed in the healthy tissue. The degradation of the collagen fibers was also confirmed by the OCT phase retardance image (see Fig. 7B). The PSOCT image showed negligible changes in phase retardance between the epidermal and dermal layers, suggesting some degree of destruction in the collagen structure.

#184392 - $15.00 USD Received 29 Jan 2013; revised 13 Mar 2013; accepted 18 Mar 2013; published 8 Apr 2013

As a control to RCM and OCT findings, the metabolic activity of the healthy and injured specimens was testing using an MTT assay [41]. Viable tissues convert the MTT to a purple dye, as shown in the photograph from Fig. 8. This is the result of the interaction of the dye with the mitochondria. The apoptotic proteins that target mitochondria cause mitochondrial swelling through the formation of membrane pores, or they may increase the permeability of the mitochondrial membrane and cause apoptotic effectors to leak out.

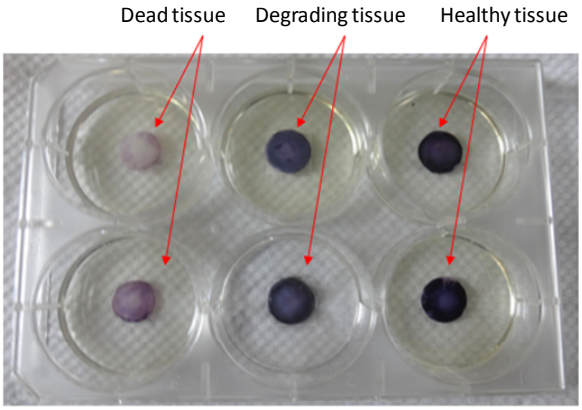

Fig. 8. Testing of the skin construct viability using the MTT assay. The tissue specimens were kept in a 6-well bioreactor. Healthy specimens turn purple, while the dead ones tend to remain almost not colored.

3.2 Instrument evaluation on human skin

Combined RCM/OCT imaging was performed on the skin of the investigators. Areas with normal-looking appearance, as well as adjacent areas with superficial scars from previous micro-burns were investigated. The main goals of this study were (1) to evaluate instrument capability for detecting small changes in tissue morphology after injury, in both RCM and OCT modes, as well as for estimating burn depth, (2) to determine if RCM can detect capillary blood flow in the upper dermis, which can be used as an indicator of tissue perfusion and therefore of its viability.

In Fig. 9 is shown an example of a minor scar on the ventral side of the finger after a superficial burn injury. The structural OCT image (Fig. 9A) shows high scattering of the light from the top of the epithelial layer of the burned area, up to a depth of about 100 μm, which indicates severe degradation in tissue morphology. Although OCT can clearly show the depth of the scar, it cannot resolve tissue morphology at the cellular level and thus it cannot be used to determine if the intracellular morphology was affected. RCM however, can be used to complement OCT findings and visualize tissue morphology at the subcellular level. For example, the RCM images show clear differences in cell morphology between the burned and the normal areas of the skin. The burned location (Area I), shows complete degradation of the cell morphology in the upper epidermis, to a depth of about 50 μm, and normal morphology deeper, demonstrating normal skin integrity in the lower epidermis and upper dermis. The RCM images of the normal tissue (Area II) show cobblestone-like cells in the upper epidermis (25 μm depth), larger polygonal cells at about 50 μm depth, slightly smaller polygonal cells with dark nuclei and bright cytoplasm at about 100 μm depth, and dermal papillae at about 200 μm depth.

Besides morphological information, both OCT and RCM can be used to get some insight about tissue functionality status. For example, OCT can be used to monitor collagen integrity, while RCM can be used to monitor tissue perfusion. The OCT birefringence (phase retardance) map (Fig. 9B), provides information regarding to collagen integrity in the dermal layer. Since the dermal layer was not affected by burn, the collagen structures remained intact

#184392 - $15.00 USD Received 29 Jan 2013; revised 13 Mar 2013; accepted 18 Mar 2013; published 8 Apr 2013

and therefore no notable loss of birefringence is observable in the phase retardance map on the dermal layer beneath the burn scar. A degradation of collagen will indicate that the dermal layer was severely affected and therefore it might not recover even with adequate therapy. Therefore, PSOCT will offer the clinician with a diagnostic tool that will help in his decision if skin grafting is needed or not.

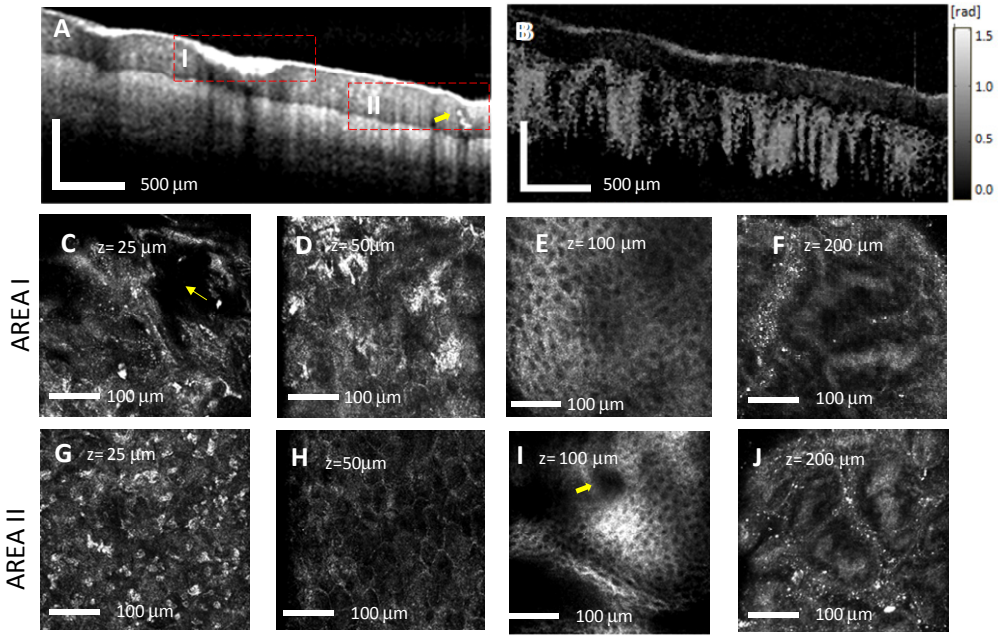

Fig. 9. OCT/RCM images from the palm of the principal investigator. (**A**): cross-sectional OCT image; (**B**): birefringence map; **Area I (C to F)**: RCM images at various depths on the scar location, showing complete degradation of cell morphology in the upper epidermis, to a depth of about 50 µm, and normal skin in the lower epidermis and upper dermis. Well differentiated polygonal cells, 10 to 20 µm in size, with dark nuclei and bright and thin cytoplasm are visible at 100 µm depth in (E), while dermal papillae are shown in F. **Area II (G to J)**: RCM images at various depths on the normal skin. Cobblestone appearance of the corneum layer cells is readable in (G), while well differentiated polygonal cells, 10 to 20 µm in size, with dark nuclei and bright and thin cytoplasm are shown in H and I. Yellow arrows indicate the presence of the sweat glands.

Besides examining the structural integrity of the tissue, burn clinicians also need to estimate skin viability in order to determine the necessity for grafting. Unfortunately, visual inspection and high-resolution imaging with a camera are not reliable in making this determination. Laser Doppler perfusion is a more promising tool, but still provides false negatives, mainly due to specular reflections, which are stronger on the burned areas than on the normal tissue due to the application of ointments. In addition, it has been reported that the distance between the scanner and skin influences the perfusion signal, which makes the measurement less reliable [35].

Doppler OCT is another tool that can be used to monitor skin perfusion. Initial work performed by other groups showed that reliable Doppler measurements were obtained only in the lower dermis, at depths higher than 500 µm [42,43]. This was caused by the fact that phase signal changes caused by the blood flow in the microcapillaries are very small, close to the noise floor. Later on, work performed by Vakoc et al. showed that the sensitivity of phase resolved OCT can be improved by processing the phase variance between adjacent B-scans [44]. However, blood flow in the upper dermis was not demonstrated until recently by Wang's group at the Oregon Health & Science University, which used an optical micro-angiography (OMAG) technique [45,46]. Their approach for resolving microcapillary blood flow in the

#184392 - $15.00 USD Received 29 Jan 2013; revised 13 Mar 2013; accepted 18 Mar 2013; published 8 Apr 2013

upper dermis was to decrease the A-line density while increasing the B-scan density, and thus the OMAG algorithm has been applied on C-scan direction rather than B-scan direction, which is the conventional approach.

Our approach was to use RCM capability for visualizing microcapillary blood flow in the upper dermis. The advantage of this approach is that blood flow can be observed without the need for additional data processing. The drawback is that deeper blood flow cannot be retrieved due to the limited penetration depth of RCM. RCM capability for visualizing microcapillary blood flow was evaluated in normal subjects only because imaging on burn injured patients was not possible with a benchtop setup in a laboratory setting. RCM movies were recorded from the forearm and the palm of the investigators. Capillary blood flow was visualized in the palm at about 250 μm depth and in the ventral side of the forearm at about 200 μm depth. For illustrative purpose only, about 50 frames from the RCM movies were used to calculate the standard deviation (SD) of each pixel and depict the capillary blood presence in the RCM image. The SD of pixel movement was different than zero in the areas where capillary blood flow was present. Thus, by attributing different colors to pixels, function of the SD value, a color display was used to display blood flow in the microcapillaries (see Fig. 10). Blue color was attributed to the large majority of the pixels where the SD was close to zero, while red was attributed to highest SD values, which correlated to the highest blood flow.

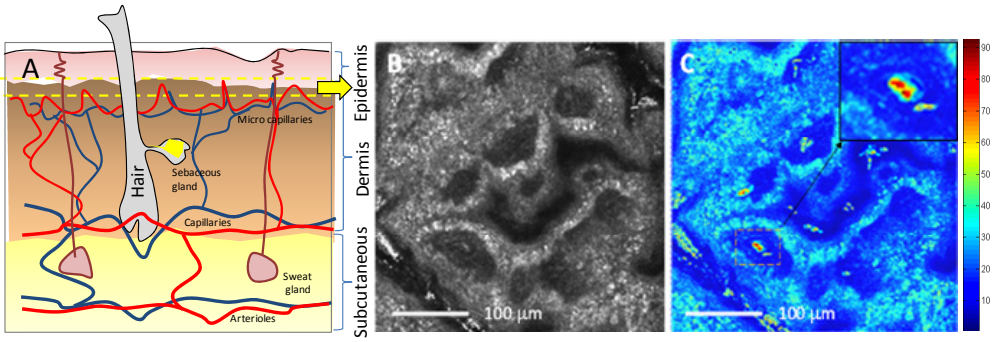

Fig. 10. (**A**): Cartoon of the skin structure highlighting the vascular network. The yellow marked areasuggests the RCM measurement site. (**B**): Selected movie frame showing an RCM image of the upper dermis; (**C**): Processed RCM frames highlighting the presence of microcapillary blood flow (see magnified ROI in (C)).

4. Discussion and conclusions

The purpose of this study was mainly to evaluate the benefit of multimodal imaging, RCM combined with OCT, for skin burns diagnosis. A dual-modality high-resolution imaging instrument was developed and preliminarily tested with the goal of investigating the hypothesis that spatially co-registered RCM/OCT images might offer a more complete picture of wound gravity in burned skin. Initial measurements on EpiDerm^{FT} skin constructs and the skin of several volunteers with minor burn-originated scars showed that indeed these two imaging modalities complement each-other and therefore might help clinicians to more reliably diagnose wound gravity. OCT helped to visualize deeper burn injuries and determine dermal damage by quantifying collagen destruction, while RCM provided submicron details of the integrity of the epidermal layer and identified the presence of the superficial blood flow.

The preliminary results of our study were quite promising, suggesting the feasibility of the proposed approach for skin burns diagnosis. However, additional efforts are needed to improve the technology and make it more appealing for clinical use. Improvements on both RCM and OCT imaging channels of the instrument are needed. For example, the imaging

#184392 - $15.00 USD Received 29 Jan 2013; revised 13 Mar 2013; accepted 18 Mar 2013; published 8 Apr 2013

depth with RCM was limited to about 250 μm, which did not allow for visualizing blood flow in areas where the epidermis was thicker (e.g., ventral side of the finger). Fortunately, the use of a relatively longer wavelength (915 nm or 1050 nm), should allow for increasing RCM imaging depth, since tissue scattering decreases with wavelength increase. Moreover, when the epidermis is visibly compromised, the clinician usually shaves it and thus RCM imaging depth might be sufficient to visualize capillary blood flow within the upper dermis.

Some limitations were observed in the OCT part of the instrument. One of the major issues was the instability of the phase between successive A-lines, which is an inherent issue to any swept-source (SS) based OCT scheme. This phase instability translates to a phase noise in the processing scheme, which severely limits the ability to estimate very small phase retardations in birefringent specimens. Improved but more expensive schemes are currently used by other investigators, such that the sample is probed with two orthogonally polarization states of the light within the same A-line [47]. Thus, very small phase retardation changes can be calculated even with a SS-OCT scheme. However, such OCT instruments are very complex and thus expensive, which might make them prohibitive for clinical use. Our alternative approach is to use a spectrometer-based system, where two spectrometers will be used in a polarization sensitive detection scheme, similar to the approach taken by D. Stifter et al. [48].

Another issue with the OCT scheme used in this study was the polarization mode dispersion (PMD) inserted by the optical circulators. The PMD induced by circulators or even moderate lengths of optical fiber, is known to be a dominant source of noise in fiber-based PS-OCT systems. Recent work performed by Zhang et al. [47,49] shows that by using a numeric PMD compensation method the PMD effects on the birefringence map can be corrected to some extent.

Our hypothesis that multimodal imaging may enable improved diagnosis is in agreement with the findings of other research groups. For example, the integration of optical coherence microscopy (OCM) and multiphoton microscopy (MPM) [40] has clearly shown the benefit of multimodal imaging for evaluating skin conditions: OCM provided cellular morphology details in reflectance mode, while MPM, in autofluorescence mode, provided increased specificity for clinically important details such as, for example, the intra-cytoplasmic distribution of proteins (keratin) and pigment (melanin) in skin. Challenges in this type of instrumentation are similar to ours: high numerical aperture (NA) for cellular-level MPM whereas lower NA for OCM; however, the use of two different beams allows for independent control of NAs. For clinical utility however, when monitoring burns, the “added value” of combined reflectance and autofuorescence vis-a-vis each individual mode is not immediately obvious and will need to be further investigated. Depending on the required level of contrast specificity, one may simply use either mode. By comparison, our motivation and approach is different: the use of OCT is for deeper imaging in the dermis, allowing for both morphological and birefringence data, which is clearly complementary to the superficial imaging of the epidermis with RCM.

A different approach was taken by other investigators: two separate instruments were used by other groups to study wound healing in organotypic skin-equivalent tissue models [31]. OCT findings were compared to MPM findings. OCT was used to retrieve depth information, while second harmonic generation (SHG) MPM, was used to image and analyze morphological changes with submicron resolution. MPM with the SHG approach provided more specific contrast than RCM for interrogating cellular (infiltrating fibroblast cells) and structural (collagen) morphology in the dermis. However, the integration of these two technologies within the same instrument was not demonstrated.

The RCM/OCT approach described herein is somewhat simpler and thus lower cost than an OCT/MPM approach. In addition, it is suitable to hand-held probe implementation, which could be the most attractive solution to be considered in order to make this technology translatable to clinical use. The RCM part has already been implemented into a hand-held

#184392 - $15.00 USD Received 29 Jan 2013; revised 13 Mar 2013; accepted 18 Mar 2013; published 8 Apr 2013

probe (VivaScope® 3000) by our collaborator, Caliber I. D. (formerly, Lucid), Rochester, NY). This probe was recently developed specifically for easier clinical imaging on harder accessible areas of the skin. We are currently working towards integrating an OCT imaging channel within the same probe. In addition to hand-held probe implementation, other important features for a clinical instrument should include high frame rate imaging to minimize motion artifacts, acquisition of image stacks at different depths in the RCM mode and raster images in the OCT mode. All these technological challenges are currently being investigated by the PSI-Caliber team with the scope of developing an improved instrument that will be suitable for clinical trials.

Acknowledgments

The authors would to tank Dr. Ben Vakoc from Wellman Center of Medicine, MGH, for this support in performing some of the preliminary PSOCT measurements.

The work of the authors was supported by the Department of Defense through Grant Number W81XWH-11-C-0486 and partially through NCI Grant Number 1R43CA162561-01A1.

Ellen Ziyi Zhang was supported by the Center for Biomedical OCT Research and Translation through Grant Number P41EB015903, awarded by the National Center for Research Resources and the National Institute of Biomedical Imaging and Bioengineering of the National Institutes of Health.

#184392 - $15.00 USD Received 29 Jan 2013; revised 13 Mar 2013; accepted 18 Mar 2013; published 8 Apr 2013